PCCP

PAPER

View Article Online
View Journal | View Issue

Cite this: *Phys. Chem. Chem. Phys.*, 2020, **22**, 9967

Hygroscopic properties of NaCl nanoparticles on the surface: a scanning force microscopy study†

Xiaoxiang Wang,‡[a] Haozhi Lei,‡[b] Rüdiger Berger, *[c] Yi Zhang, [b] Hang Su[a] and Yafang Cheng *[a]

Received 10th January 2020,
Accepted 8th April 2020

DOI: 10.1039/d0cp00155d

rsc.li/pccp

We investigated the hygroscopic growth of sodium chloride (NaCl) nanoparticles with curvature related diameters ranging from 10 nm to 200 nm, at different relative humidities using scanning force microscopy. Hygroscopic aerosol nanoparticles play a vital role in the Earth's climate and human health. We report that 10 nm NaCl nanoparticles adsorbed on silicon surfaces have a higher deliquescence relative humidity than larger NaCl nanoparticles (size > 30 nm). This finding is consistent with the observations for airborne nanoparticles by hygroscopicity tandem differential mobility analyzer. Therefore, the presence of silicon surfaces plays no significant role in the deliquescence relative humidity. Moreover, the study of individual airborne particles by means of scanning force microscopy revealed that the ability of water uptake, *i.e.* growth factor, of NaCl particles differs by as large as 40% at the same relative humidity. This finding indicates that the individual nature of NaCl particles influences the growth factor.

Introduction

Nanoparticles are a significant component of atmospheric aerosols. Aerosols are proposed to influence the Earth's climate and human health.[1–4] Often, atmospheric aerosols are hygroscopic, and they can grow significantly in humid environments.[5,6] Therefore, studying the hygroscopic properties of the suspended atmospheric nanoparticles at different relative humidities (RH) has received significant attention.[7–10] In particular, the phase state of the atmospheric nanoparticles determines their optical properties, cloud-droplet nucleation efficiency and heterogeneous chemistry.[11–16] Details of the phase transition at different humidities can be inferred from the analysis of hygroscopic growth curve of individual aerosol particles or aerosol populations.

Atmospheric aerosols can adsorb water on surfaces,[17,18] and the hygroscopic property of the adsorbed nanoparticles may influence chemical and physical processes on the surface. Substantial water sorption by nanoparticles may lead to surface corrosion, which is a serious problem for electronic devices.[19] Therefore, the behaviors of nanoparticles on surfaces at different humidities have been studied intensively. Ghorai and Tivanski used X-ray microscopy (STXM) and near-edge X-ray absorption fine structure (NEXAFS) spectroscopy to investigate atmospherically relevant NaCl, NaBr, NaI and $NaNO_3$ nanoparticles on Si_3N_4 windows.[20] Freney *et al.* checked the phase state of mixed aerosol particles consisting of one or more hygroscopic compounds at different RHs by using a transmission electron microscope operated with an environmental cell (ETEM).[21] Recently, Morris *et al.* used a scanning force microscope (SFM) to measure the surface area and volume equivalent diameter of NaCl nanoparticles, and malonic acid (MA) nanoparticles with binary mixtures at different RHs.[22] Bondy *et al.* analyzed infrared spectra recorded using an SFM on nanometer-sized atmospheric model systems.[23]

However, the role of the surface on the response of aerosol nanoparticles to humidity is still not clear. Eom *et al.*[24] examined the hygroscopic properties of micrometer-sized inorganic particles on different types of substrates using optical microscopy. They found that the substrate has no influence on the deliquescence relative humidity (DRH) of these micrometer-sized particles.[24] The DRH is the relative humidity (RH) value corresponding to the phase transition from a solid to a liquid.[25] In contrast, Morris *et al.* reported that NaCl particles with slightly smaller diameters of 0.5–1 μm on the surface exhibit a different growth behavior compared to airborne particles upon exposure to humidity.[22] In addition, the shape and size of particles varies at different RHs.[26] The latter was measured by using a humidified tandem differential mobility analyzer (HTDMA). These measurements indicate that the diameter of the particles is not the only parameter that controls the growth factor. It seems likely that the morphology and shape of particles play a role in the growth behavior, too. Consequently, methods allowing one to measure the size and shape dependence of the hygroscopicity of nanoparticles

[a] *Max Planck Institute for Chemistry, Multiphase Chemistry Department, Hahn Meitner Weg 1, 55128 Mainz, Germany. E-mail: yafang.cheng@mpic.de*
[b] *Key Laboratory of Interfacial Physics and Technology, Shanghai Institute of Applied Physics, Chinese Academy of Sciences, Shanghai 201800, China*
[c] *Max Planck Institute for Polymer Research, Ackermannweg 10, Mainz 55128, Germany. E-mail: berger@mpip-mainz.mpg.de*

† Electronic supplementary information (ESI) available. See DOI: 10.1039/d0cp00155d

‡ Xiaoxiang Wang and Haozhi Lei contributed equally to this work.

are required. In particular, aerosol nanoparticles <100 nm on surfaces have not been studied, although these particles may be more important for climate change and human health than larger ones.[3,27,28]

In this study, NaCl particles, which are one of the most important components of atmospheric aerosol particles,[29,30] were chosen. Particles with different sizes were generated and collected onto a silicon substrate. In particular, we focused on small particles with mobility diameters D_{mobility} of 200 ± 15 nm, 30 ± 2 nm and 10 ± 0.5 nm, which may be prone to surface effects more than particles >200 nm.[8,31] The error in sizes is given by the DMA transfer function. The morphology and hygroscopic growth at different RHs were analyzed by using SFM. Based on SFM parameters, we calculated the volume of NaCl particles and we introduce a model to calculate the curvature related diameter ($D_{\mathrm{curvature}}$). Changes in $D_{\mathrm{curvature}}$ upon humidity exposure allowed us to determine the DRH of different particle sizes. The data from this study was compared to the values for suspended particles from HTDMA. This comparison confirms results of the previous theory about the nano-size effect on particle phase transition[9] and indicates that the method developed for airborne nanoparticles applies to the deliquescence of nanoparticles on surfaces as well.

Methods and materials

Generation and collection of NaCl aerosol nanoparticles

Sodium chloride (NaCl) was purchased from Sigma-Aldrich (reagent grade, 99.99% purity) and prepared in deionized water (18 MΩ cm). The aqueous solution containing NaCl was atomized using a TSI 3076 constant output atomizer (TSI, Inc.), and dried ($\sim$5% RH) by passing through a diffusion silica dryer. The aim of our study is to measure size dependent hygroscopic properties of particles attached to a surface. Thus, the dehydrated aerosol particles with different values of D_{mobility} were selected using a differential mobility analyzer (DMA; TSI, Inc. Model 3081A) and then deposited on silicon substrates (Ted Pella Inc., Part No. 16008) *via* impaction using a pump running with a flow of 1.5 L min^{-1}. Prior to the sampling, the silicon substrates were cleaned in Argon plasma for 2 min. The mobility diameters of the NaCl particles that we collected for later SFM measurements are monodispersed particles with a peak diameter at 200 nm, 30 nm and 10 nm. A flow diagram of all preparation steps is shown in Fig. 1a.

Scanning force microscopy analysis

All SFM data were obtained in a tapping mode by adjusting the minimum force between the tip and the sample while imaging (Dimension Icon, Bruker). Silicon substrates with deposited nanoparticles were placed in a custom made SFM Teflon cell (Fig. 1b and c). This cell has a volume of 25 cm^3 and allowed us to adjust the RH during the SFM measurements with a precision of $<5\%$.[26] Silicon cantilevers (OMCL-AC240TN-R3, OLYMPUS) with a nominal spring constant of 2 N m^{-1} and a nominal tip radius of 7 nm were used. The half angle of probe's conical

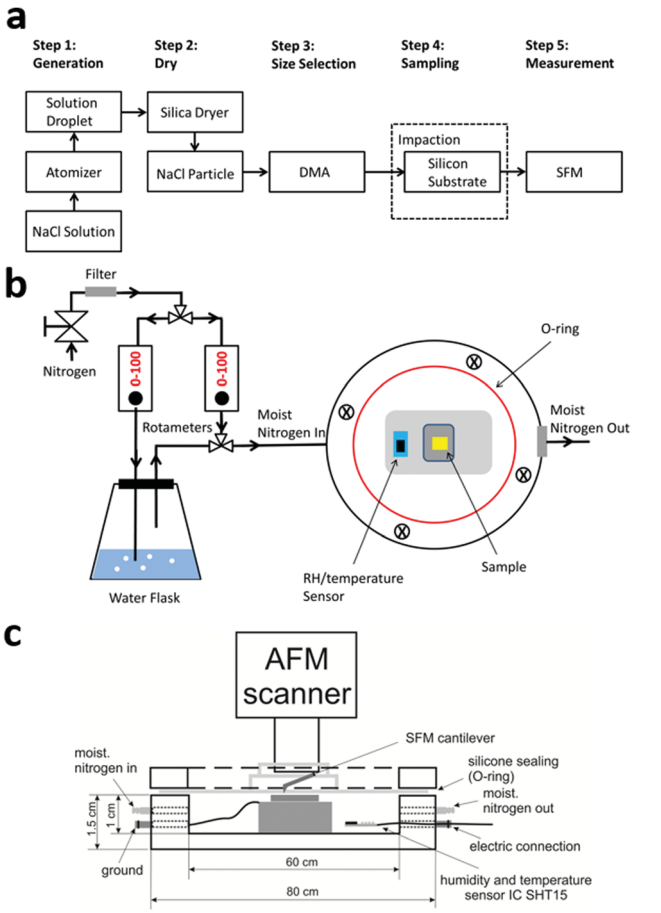

Fig. 1 The experimental process in this study. (a) A flow diagram of the sequence of steps. (b) Details of the setup in the SFM measurements; one gas line bubbles through water. The humidified nitrogen is then mixed with dry nitrogen. With the two rotameters, we adjust the mixing ration of humidified and dry gas. The SFM-tip including a sombrero-shaped gas tight silicone seal is lowered from the top. (c) A side view of the homebuilt SFM Teflon cell.

angle is about 17.5°.[32] The SFM analysis started at an initial RH of $\sim$5%, followed by gradual increases until the RH reached 90%. After adjusting one RH value by flow controllers (rotameters), an equilibrium RH was reached within 10–15 minutes in the Teflon cell. The SFM images of the particles were then recorded at each RH, respectively. After increasing the RH, we decreased the RH again in order to check the reversibility and stability of the particles. The raw SFM data were analyzed using the NanoScope Analysis 1.5 package.

Quantifying the size of nanoparticles and DRH

Different parameters have been used to quantify the sizes of airborne particles (aerosol) and deposited particles. The parameter D_{mobility} is given by the diameter of a particle with the same electrical mobility.[33,34] Alternatively, the Stokes diameter (D_{Stokes}), which is the diameter of a sphere with the same terminal settling velocity and density as the particle, was also used.[34] In addition, the volume equivalent diameter (D_{volume}) of non-spherical particles was used to quantify the size of deposited

particles at different RHs in previous SFM studies.[22,35] The D_{volume} is equal to the diameter of a spherical particle which exhibits an identical volume. Principally, all the above parameters are reasonable for quantifying the hygroscopic growth of particles. Therefore, we have analyzed the volume of particles at different RHs based on SFM measurements. However, this parameter does not reflect changes in the shape. Many physical properties of nanoparticles are caused by changes of its surface properties, such as curvature, but are not solely dependant on the change in its volume.[36,37] For example, the equilibrium between water vapor and solution droplet is strongly affected by the curvature of the nanoparticle surface.[38] Additionally, in order to address changes in shape with a single parameter, we used a curvature related diameter $D_{curvature}$ to quantify the size of particles (Fig. 2a). In order to calculate $D_{curvature}$ of particles, we measured the height of particles, h. The lateral elongation of particles, L, is calculated by considering SFM-tip convolution effects. In particular, the size and phase of particles determine the degrees of overestimations of L (Fig. 2b–e). In our analysis, we approximated the tip apex shape with a semi-sphere having a radius of 10 nm followed by a cone with an opening angle of 35°[32] (Fig. 2b). When the height of a solid particle is higher than the radius of the tip, the edge of the cone touches the particle (Fig. 2c). In this case, we use

$$L = L_m - 2h\cdot\tan 17.5^\circ \quad (1)$$

to calculate L. L_m is taken from a line-profile across the particle. It is the distance between the points, which elevates from the substrate plane. When the height of a solid particle is lower than the radius of the tip, we use

$$L = L_m - 20\ \text{nm} \quad (2)$$

to calculate L (Fig. 2d). After the deliquescence, the particles are in a liquid state (Fig. 2e). In this case, we also use eqn (2) to calculate L no matter what size it is. After calculating L for particles with different sizes, we calculated $D_{curvature}$ using a geometrical model:

$$D_{curvature} = h + \frac{L^2}{4h} \quad (3)$$

In particular, the calculation of the shape-related diameter $D_{curvature}$, as defined here, reflects geometrical changes given by the transition from a crystalline (Fig. 2a) into a liquid state (Fig. 2e), although the volume remains unchanged. Therefore, solid–liquid transitions should appear more clearly compared to the analysis of volume changes. We consider these curvatures as first order changes. Second order changes are attributed to a variation of the curvature along different directions of particles as they are not perfectly symmetrical, and to local curvatures of the particle surfaces (Table S1, ESI†). To calculate the volume of dry particles, we use

$$V = L^2\cdot h \quad (4)$$

as these particles are cuboids. Particles become spherical caps after the deliquescence, and thus we use

$$V = \frac{1}{6}\pi\cdot h\cdot\left(h^2 + \frac{3L^2}{4}\right) \quad (5)$$

to calculate the volume.

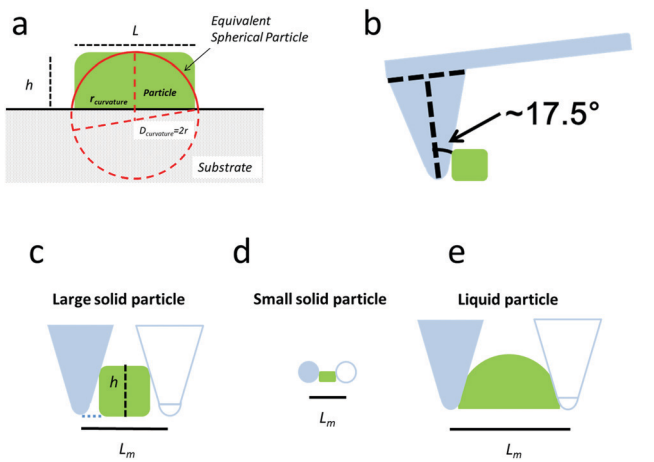

Fig. 2 Schematic diagram for the calculation of the curvature related diameter. (a) The green box represents the NaCl particle, and "L" is its horizontal length, and "h" is its height. (b) The probe and tip contact the particle studied. (c) In this case, the particle studied touchs the probe during the measurement, "L_m" contains double of h·tan17.5° (dashed blue line). So "$L_m - 2h$·tan17.5°" can represent L. (d and e) $L = L_m - 20$ nm.

Results and discussion

Distribution and morphology

Aerosol particles ($D_{mobility}$ 10 nm, 30 nm or 200 nm) deposited on silicon substrates were imaged by SFM at a RH of 5% firstly. At this condition, the heights of particles range between ~10 nm and ~200 nm (Fig. 3a). These height values correspond to the $D_{mobility}$ size range of particles that we adjusted with the differential mobility analyzer. Up to a RH of 60%, no changes of position or shape of the particles were detected after repeated SFM scans (Fig. 3b–d).

10 nm particles. When the RH reached about 75%, the particle with a height of ≥30 nm still remain unaltered on

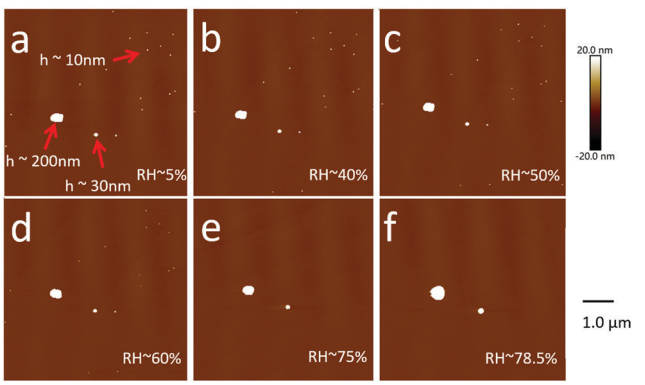

Fig. 3 SFM images of NaCl particles with different sizes on the same substrate at different RH conditions. The corresponding phase contrast images are provided in the ESI† (Fig. S1).

the surface (Fig. 3e). However, the particles with a height of ~10 nm disappeared after the first scan (Fig. 3e). After increasing the RH to 78.5%, particles which disappeared were still not being found (Fig. 3f). One possibility is that the SFM-tip while scanning sweeps these particles away. However, we could not find traces of particles at the edge of the scan window. Another possibility would be that these small particles are dissolved by water that forms a meniscus between the particles and the surface, *e.g.*, due to Kelvin equation.[39] Weeks *et al.* observed by environmental scanning electron microscopy that such a water meniscus starts to form at RH > 70% between a Silicon-nitride SFM-tip and a Silicon substrate.[39] The appearance of such a water meniscus at a RH > 70% coincides with our observation that small NaCl particles disappear at a RH of 75%. In addition, it is noteworthy, that several previous studies of hygroscopic NaCl particles using SFM were all limited to particle diameters larger than hundreds of nanometers at different RH conditions.[22,24,40,41] Thus, it might be impossible to image such small airborne NaCl particles at a RH > 70% by SFM due to the formation of a water meniscus between the particle and the substrate and/or between the particle and the SFM-tip. Although the exact mechanism is unclear, the reason for the disappearance of airborne NaCl particles with a $D_{mobility}$ of ~10 nm is the increase in RH above 70%.

30 nm particles. The slightly larger particles which correspond to a $D_{mobility}$ of 30 nm could be imaged above a RH of 75% (Fig. 3d). The size of the particles increases, and the phase becomes liquid at a high RH. After decreasing the RH, we found that the particles are attributed to a $D_{mobility}$ of 30 nm (Fig. 4a) and decreased in height to <10 nm (Fig. 4b). It is possible that some of the liquid was removed by scanning the SFM-tip leaving a smaller fraction of NaCl behind. These residual NaCl particles exhibit a height of ~4 nm at 10% RH. Correspondingly, its $D_{curvature}$ is ~10 nm. These small particles are immobile on the surface and possibly adhere much stronger to the surface as they were in a liquid state before (Fig. 5a). A subsequent stepwise increase in RH again to 90% leads to an increase in size until finally they became round at a RH of 90% (Fig. 5b). Interestingly, these small particles can be imaged reproducibly by SFM, which is different from the case of 10 nm particles from DMA directly; they do not disappear. It is possible that adhesion of such particles is much stronger. We hereby use these residual NaCl particles to study the hygroscopic growth $D_{curvature}$ at ~10 nm.

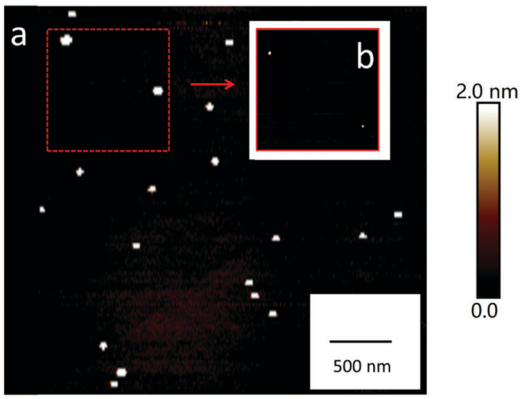

Fig. 4 (a) SFM micrograph of particles at a RH of ~20% directly after preparation. Particles which correspond to a $D_{mobility}$ of 30 nm can be measured. (b) The identical area in the red dashed box of panel (a) after exposure to a RH of 90%. Now, residual particles from an NaCl particle with an initial $D_{mobility}$ of 30 nm were measured. These residual particles exhibit a $D_{curvature}$ of ~10 nm.

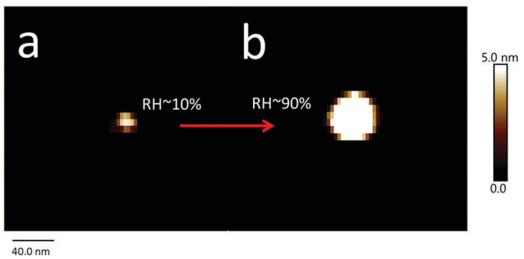

Fig. 5 SFM images of one NaCl particle with a $D_{curvature}$ of ~10 nm. (a) SFM topography image of a residual NaCl particle with a $D_{curvature}$ of ~10 nm imaged at a RH of ~10%. (b) The same NaCl particle imaged at a RH of ~90%. At this RH, the round particle is a deliquesced NaCl solution droplet.

200 nm particles. Next, we recorded images of larger particles to examine the change of morphology of particles. Firstly, the morphology of a cuboid NaCl particle with L of 210 nm (RH ~ 5%) was analyzed (Fig. 6a). This particle corresponds most likely to one of the particles with a $D_{mobility}$ of 200 nm. It retains a cuboid shape with corners that are rounded. Rounded corners were also observed by Bruzewicz *et al.* using non-contact environmental SFM.[41] Using eqn (3), we calculated a $D_{curvature}$ of 208 nm. For such large NaCl particles, a DRH of 75% was determined by HTDMA.[7,42] Therefore, the SFM exhibits a clear shape change of the cuboid NaCl particle into a semi-spherical object at a RH of 90% (Fig. 6b). The semispherical shape indicates the formation of a liquid droplet on the surface. Correspondingly, we calculated an increase in $D_{curvature}$ to 543 nm. This interpretation is supported by the simultaneously recorded phase variation of the oscillating SFM cantilever (Fig. S1, ESI†).

To summarize, we can image and analyze NaCl nanoparticles with a $D_{curvature}$ from 10 nm up to 772 nm and at a RH from 5% up to 90%. Next, we analyzed the $D_{curvature}$ changes in dependence of RH in more detail with the aim to calculate the growth factors (GFs) and the deliquescence relative humidity (DRH).

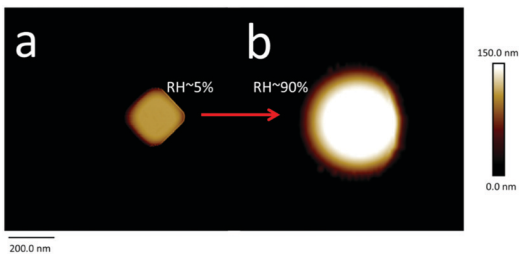

Fig. 6 SFM images of one NaCl particle with a $D_{curvature}$ of ~200 nm. Images are shown in height mode here. (a) Image at the RH of ~5%. The particle is solid. (b) Image at the RH of ~90% ($D_{curvature}$ of ~540 nm). The round particle is supposed to be a deliquescent NaCl solution droplet.

Growth factor and deliquescence relative humidity

The growth factor (GF_C) of particles can be defined by

$$GF_C(RH) = \frac{D_{curvature}(RH)}{D_{curvature}(\text{lowest RH})} \quad (6)$$

where $GF_C(RH)$ is the GF at a particular RH, $D_{curvature}(RH)$ is the calculated curvature related diameter at a particular RH (eqn (3)), and $D_{curvature}$(lowest RH) is the curvature related diameter at the lowest RH (5–20%) studied for the corresponding particle. Here we plotted the GF_C of two populations of particles, *i.e.*, $D_{curvature}$ ~ 200 nm and ~10 nm (Fig. 7a). In addition, GFs from HTDMA measurements for particles with a $D_{mobility}$ of 100 nm and 10 nm at different RH conditions were plotted for comparison, as well as curves based on the Köhler theory.[7,9,42] For comparison, we also calculated the GF based on the change of volume of particles (GF_V) by using eqn (7),[22,43] and the results are presented (Fig. 7b) and discussed below.

$$GF_V(RH) = \sqrt[3]{\frac{V(RH)}{V(\text{lowest RH})}} \quad (7)$$

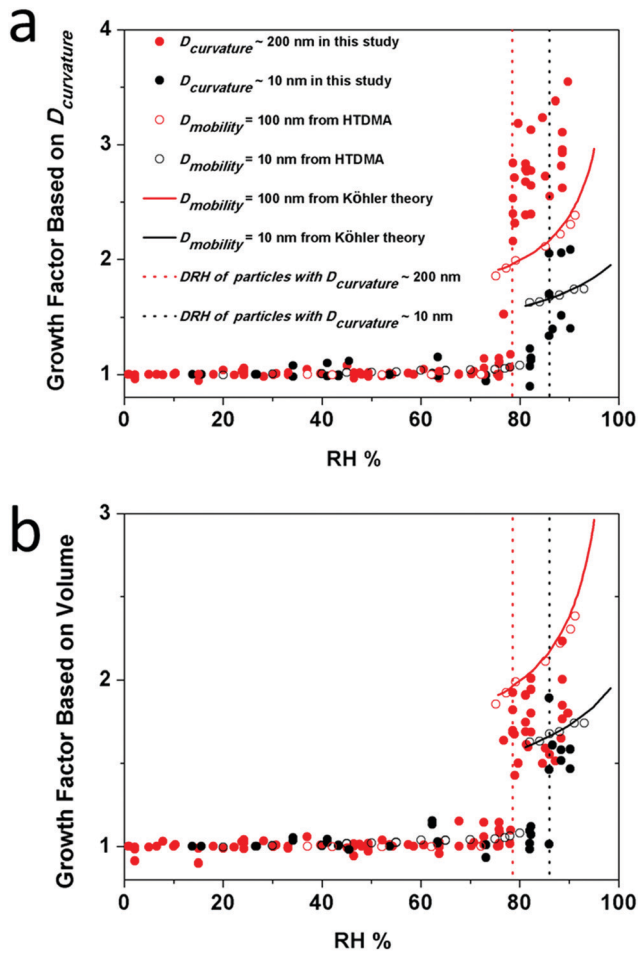

Fig. 7 Hygroscopic growth curves of NaCl based on the $D_{curvature}$ (a) and the volume (b). Red solid circles, red open circles, black solid circles and black open circles represent the growth factor of particles with a $D_{curvature}$ of ~200 nm, $D_{mobility}$ = 100 nm, $D_{curvature}$ of ~10 nm and $D_{mobility}$= 10 nm at different RHs. Solid lines represent hygroscopic growth factors calculated based on the Köhler theory. Dashed lines indicate the DRH of particles with a $D_{curvature}$ of ~200 nm and ~10 nm. For larger particles, *i.e.*, $D_{curvature}$ of ~200 nm, we measured 7 individual ones. For smaller particles, *i.e.*, $D_{curvature}$ of ~10 nm, we measured 5 individual ones (Tables S2–S5 in the ESI†).

For the population of particles with a $D_{curvature}$ of ~200 nm, we calculated GFs of about 1 up to a RH of 77% (Fig. 7a). The RH at which nanoparticles become significantly larger is defined as the DRH. For particles with a $D_{curvature}$ of ~200 nm, we measured a steep increase of the GF_C at a RH of 78 ± 1%. This RH corresponds to the DRH and is indicated by a red dashed line in Fig. 7. For the population of particles with a $D_{curvature}$ of ~10 nm, we measured a constant growth factor of 1 up to a RH of 86 ± 1% which is 8% higher in RH compared to the particles with diameters of ~200 nm. After a RH of 86 ± 1%, a significant increase in the GF_C to values >1.5 was observed. The DRH of particles with a $D_{curvature}$ of ~10 nm corresponds to 86 ± 1% (black dashed line in Fig. 7). Our measurements indicate that the GF for larger particles are higher than the GF for smaller particles at the same RH conditions after the deliquescence. This observation also holds for the GFs, which are calculated by the volume change (Fig. 7b). For the population of larger particles, GFs are about 1 up to a RH of 77% (Fig. 7b). For these particles, we measured a steep increase of the GF_V at a RH of 78 ± 1%. This RH is the same as determined by the GFs through the curvature analysis. For the population of smaller particles, we measured a constant growth factor of 1 up to a RH of 86 ± 1%. Here, the corresponding DRH value is consistent with our analysis of the curvature as well. In particular, both DRH values are consistent with the results from HTDMA methods for airborne particles.[7]

Notably, the magnitude of the GF calculated by volume changes is in good agreement with the HTDMA data (Fig. 7b). However, the GF magnitude calculated by the curvature related diameter is significantly higher for 200 nm-sized NaCl nanoparticles. The latter probably indicate that the calculation of $D_{curvature}$ accentuates changes from a crystalline state into a liquid state, where the solid to liquid phase transition could be resolved more clearly. The calculation $D_{curvature}$ of the latter is enabled by using an imaging technique where the height and the width of nano-scale particles can be measured.

The SFM method allowed us to analyze different particles of almost the same $D_{curvature}$. Interestingly, the GF of particles with the same $D_{curvature}$ can be different at the same RH. For example, at a RH of 77%, GFs of different particles with a $D_{curvature}$ of ~200 nm vary from 1.5 to 3.2 (Fig. 7a). For comparison at a RH of 77%, the GF_V varies only from 1.4 to 1.9. Therefore, different NaCl nanoparticles exhibit different abilities for water uptake. In other words, the parameter of $D_{curvature}$, as well as the volume, does not solely define the growth factor of the particles, and the population of particles with the same $D_{curvature}$ may behave differently. This difference has been rarely reported so far because the HTDMA method yields an ensemble with an average of thousands of particle

measurements. SFM allows us to study individual particles, though at a significantly reduced statistic.

The HTDMA method revealed a DRH of ~87% and ~75% for airborne particles with a $D_{mobility}$ of 10 nm and 100 nm, respectively.[7,42] Both DRH values are not much different from those measured for smaller and larger particles on surfaces, *i.e.*, 86 ± 1%, and 78 ± 1%. Therefore, we conclude that the substrate has a negligible influence on the DRH of NaCl nanoparticles down to a size of 10 nm. This conclusion is in agreement with the findings of Eom *et al.* who reported that the substrate has no influence on the DRH of micrometer-sized particles.[24] In addition, the size dependence of the DRH of nanoparticles, *i.e.*, DRH increases as the size decreases, was explained in our previous study,[9] and the same size dependence was confirmed here in this study. Therefore, we conclude that the theory developed there to explain the size dependent phase transition for airborne nanoparticles and the Differential Köhler Analysis (DKA) can be applied to the NaCl nanoparticles on the surface as well.

Summary

Previously, experimental and theoretical studies have reported a change of DRH for airborne particles of different sizes.[7,9,25,44,45] For airborne NaCl particles, the DRH increases by ~5% when the diameter decreases from 100 nm to 10 nm. Our measurements confirm this dependence for particles deposited on silicon surfaces. Thus, we conclude that the theory developed in our previous study[9] to explain the size-dependent phase transition for airborne nanoparticles can describe the deliquescence of airborne nanoparticles on surfaces as well.

Particles on hydrophobic surfaces at a high humidity might behave differently. Small particles on hydrophobic surfaces could be more stable. SFM is a suitable tool for comparing similar-sized airborne nanoparticle surfaces with different surface energies at a high humidity. Our study of individual nanoparticles revealed that the corresponding GFs can vary. The latter indicates that different airborne particles have different abilities for water uptake. Here, possibly, the exact shape, composition or orientation of the particle plays a role.

Conflicts of interest

There are no conflicts to declare.

Acknowledgements

This study is supported by the Max Planck Society (MPG). Xiaoxiang Wang acknowledges the support from the China Scholarship Council (CSC, 201406190170) and from the Program for Guangdong Introducing Innovative and Entrepreneurial Teams (2017ZT07Z479). Haozhi Lei acknowledges the Project-related exchange of Persons Program (201600110073) from CSC and German Academic Exchange Service. Yafang Cheng acknowledges the Minerva Program from MPG. We thank Ulrich Pöschl (MPIC) and Hans-Jürgen Butt (MPI-P) for the constructive discussions and support. We thank Michael Kappl for discussions and the design of the SFM-Teflon cell. In addition, we thank Helma Burg and Uwe Rietzler for continuous support in the SFM lab. Open Access funding provided by the Max Planck Society.

References

1 M. Kulmala and V.-M. Kerminen, *Atmos. Res.*, 2008, **90**, 132–150.
2 P. R. Buseck and K. Adachi, *Elements*, 2008, **4**, 389–394.
3 J. N. Smith, K. C. Barsanti, H. R. Friedli, M. Ehn, M. Kulmala, D. R. Collins, J. H. Scheckman, B. J. Williams and P. H. McMurry, *Proc. Natl. Acad. Sci. U. S. A.*, 2010, **107**, 6634–6639.
4 B. Nowack and T. D. Bucheli, *Environ. Pollut.*, 2007, **150**, 5–22.
5 T. Lei, A. Zuend, Y. Cheng, H. Su, W. Wang and M. Ge, *Atmos. Chem. Phys.*, 2018, **18**, 1045–1064.
6 O. H. Berg, E. Swietlicki, G. Frank, B. G. Martinsson, S. I. Cederfelt, P. Laj, L. Ricci, A. Berner, U. Dusek and Z. Galambos, *Contrib. Atmos. Phys.*, 1998, **71**, 47–64.
7 G. Biskos, A. Malinowski, L. Russell, P. Buseck and S. Martin, *Aerosol Sci. Technol.*, 2006, **40**, 97–106.
8 G. Biskos, L. Russell, P. Buseck and S. T. Martin, *Geophys. Res. Lett.*, 2006, **33**, L07801.
9 Y. Cheng, H. Su, T. Koop, E. Mikhailov and U. Pöschl, *Nat. Commun.*, 2015, **6**, 5923.
10 E. Mikhailov, S. Vlasenko, R. Niessner and U. Pöschl, *Atmos. Chem. Phys.*, 2004, **4**, 323–350.
11 S. T. Martin, *Chem. Rev.*, 2000, **100**, 3403–3454.
12 R. M. Harvey, A. P. Bateman, S. Jain, Y. J. Li, S. Martin and G. A. Petrucci, *Environ. Sci. Technol.*, 2016, **50**, 4997–5006.
13 M. Tang, D. J. Cziczo and V. H. Grassian, *Chem. Rev.*, 2016, **116**, 4205–4259.
14 M. M. Chim, C. Y. Chow, J. F. Davies and M. N. Chan, *J. Phys. Chem. A*, 2017, **121**, 1666–1674.
15 E. Mikhailov, S. Vlasenko, S. Martin, T. Koop and U. Pöschl, *Atmos. Chem. Phys.*, 2009, **9**, 9491–9522.
16 Y. Cheng, G. Zheng, C. Wei, Q. Mu, B. Zheng, Z. Wang, M. Gao, Q. Zhang, K. He and G. Carmichael, *Sci. Adv.*, 2016, **2**, e1601530.
17 B. Dahneke, *J. Colloid Interface Sci.*, 1971, **37**, 342–353.
18 J. K. Jokiniemi, T. Lind, J. Hokkinen, J. Kurkela and E. I. Kauppinen, presented in part at the Aerosols from Biomass Combustion, Zurich, Switzerland, 2001.
19 A. J. Gadgil and W. J. Fisk, *Indoor Air*, 2000, **10**, 47–56.
20 S. Ghorai and A. V. Tivanski, *Anal. Chem.*, 2010, **82**, 9289–9298.
21 E. J. Freney, K. Adachi and P. R. Buseck, *J. Geophys. Res.: Atmos.*, 2010, **115**, D19210.
22 H. S. Morris, A. D. Estillore, O. Laskina, V. H. Grassian and A. V. Tivanski, *Anal. Chem.*, 2016, **88**, 3647–3654.
23 A. L. Bondy, R. M. Kirpes, R. L. Merzel, K. A. Pratt, M. M. Banaszak Holl and A. P. Ault, *Anal. Chem.*, 2017, **89**, 8594–8598.
24 H.-J. Eom, D. Gupta, X. Li, H.-J. Jung, H. Kim and C.-U. Ro, *Anal. Chem.*, 2014, **86**, 2648–2656.
25 G. Biskos, D. Paulsen, L. Russell, P. Buseck and S. Martin, *Atmos. Chem. Phys.*, 2006, **6**, 4633–4642.

26 J. Baltrusaitis and V. H. Grassian, *J. Phys. Chem. A*, 2012, **116**, 9001–9009.
27 M. Hussain, P. Madl and A. Khan, *Health*, 2011, **2**, 51–59.
28 H.-E. Wichmann and A. Peters, *Ultrafine Particles in the Atmosphere*, World Scientific, 2000, pp. 243–267.
29 E. R. Lewis, R. Lewis and S. E. Schwartz, *Sea salt aerosol production: mechanisms, methods, measurements, and models*, American Geophysical Union, 2004.
30 B. Finlayson-Pitts, *Chem. Rev.*, 2003, **103**, 4801–4822.
31 R. McGraw and E. R. Lewis, *J. Chem. Phys.*, 2009, **131**, 194705.
32 Olympus, Micro cantilever, http://topview-photonics.com/mw/cufiles/files/EN/Olympus_AFM_Probes/datasheet/omcl-ac240tn-r3_spec_v1_2.pdf.
33 B. Y. Liu, D. Pui and A. Kapadia, *Electrical aerosol analyzer: history, principle, and data reduction*, Minnesota Univ., Dept. of Mechanical Engineering, Minneapolis, USA, 1976.
34 J. H. Seinfeld and S. N. Pandis, *Atmospheric chemistry and physics: from air pollution to climate change*, John Wiley & Sons, 2016.
35 P. Gwaze, H. J. Annegarn, J. Huth and G. Helas, *Atmos. Res.*, 2007, **86**, 93–104.
36 R. C. Tolman, *J. Chem. Phys.*, 1949, **17**, 333–337.
37 R. Kofman, P. Cheyssac, A. Aouaj, Y. Lereah, G. Deutscher, T. Ben-David, J. Penisson and A. Bourret, *Surf. Sci.*, 1994, **303**, 231–246.
38 W. Thomson, *Proc. R. Soc. Edinburgh*, 1872, **7**, 63–68.
39 B. L. Weeks, M. W. Vaughn and J. J. DeYoreo, *Langmuir*, 2005, **21**, 8096–8098.
40 O. Laskina, H. S. Morris, J. R. Grandquist, Z. Qin, E. A. Stone, A. V. Tivanski and V. H. Grassian, *J. Phys. Chem. A*, 2015, **119**, 4489–4497.
41 D. A. Bruzewicz, A. Checco, B. M. Ocko, E. R. Lewis, R. L. McGraw and S. E. Schwartz, *J. Chem. Phys.*, 2011, **134**, 044702.
42 C. N. Cruz and S. N. Pandis, *Environ. Sci. Technol.*, 2000, **34**, 4313–4319.
43 H. Yu, W. Li, Y. Zhang, P. Tunved, M. Dall'Osto, X. Shen, J. Sun, X. Zhang, J. Zhang and Z. Shi, *Atmos. Chem. Phys.*, 2019, **19**, 10433–10446.
44 K. Hämeri, A. Laaksonen, M. Väkevä and T. Suni, *J. Geophys. Res.: Atmos.*, 2001, **106**, 20749–20757.
45 R. Bahadur and L. M. Russell, *Aerosol Sci. Technol.*, 2008, **42**, 369–376.